A Wasserstein distance-based analogous method to predict distribution of non-uniform corrosion on reinforcements in concrete

Qifang Liu[a] and Ray Kai Leung Su[a*]

[a]*Department of Civil Engineering, The University of Hong Kong, Pokfulam Road, Hong Kong, China*

Abstract: This paper presents an analogous method to predict the distribution of non-uniform corrosion on reinforcements in concrete by minimizing the Wasserstein distance. A comparison between the predicted and experimental results shows that the proposed method is capable of predicting distributions of non-uniform corrosion modeled by Gaussian functions. The non-uniformity and the total area of the rust layer are selected as the key parameters to determine the distribution of non-uniform corrosion on reinforcements. Empirical equations of the non-uniformity and the total area of the rust layer versus degree of corrosion are proposed to validate the application of the method for practical projects. The method presented in this study fills a research gap in quantifying the distribution of non-uniform corrosion on reinforcements by realistically simulating crack propagation in concrete.

Keywords: non-uniform corrosion; reinforced concrete structures; distribution of rust; Wasserstein distance; analogous method.

1. Introduction

Reinforcement corrosion is one of the most important underlying reasons for the premature deterioration of reinforced concrete (RC) structures. There is a considerable volume of research work [1-8] that endeavor to investigate the crack of concrete cover due to the uniform or general corrosion of the reinforcements. However, the localized

* Corresponding author. Tel.:+852 2859 2648
E-mail address: klsu@hku.hk (RKL Su)

corrosion of reinforcements is usually observed in chloride contaminated concrete [9]. Moreover, reinforcements, for instance the corner rebar, are usually protected with a non-uniform concrete cover in buildings. As a result, the corrosion products around reinforcements are always non-uniform. According to Gonzalez et al. [9], the non-uniformity of localized corrosion, defined as the ratio of maximum corrosion penetration and the average depth of corrosion, is about three to nine. This can cause higher tensile stress and earlier occurrence of cracking in the concrete cover.

Related research efforts have been made to numerically simulate the cracking in concrete induced by the non-uniform corrosion of reinforcements [10-18]. In these studies, the distribution of rust is considered to be a crucial boundary condition and the key to obtaining a realistic stress field and corrosion cracking state.

Various models of the non-uniform corrosion of reinforcements have been developed and utilized for simulating the crack propagation in concrete covers, including the linearly decreasing model [10-12], quadratic expansion model [13], Rigid-Body-Spring Method and corrosion-expansion model [14, 15], elliptical model [16, 17, 19], Gaussian model [20, 21], and von Mises model [18]. All of the above mentioned models were developed based on limited experiments [9, 19-21] that used destructive testing methods by breaking up the concrete to measure thickness of the rust layer. However, this practice entails difficulties in measuring non-uniform reinforcement corrosion, especially for naturally corroded reinforcements because a long period of time is needed for generating sufficient amount of corrosion products to facilitate measurement [9]. Moreover, the process to prepare the specimens for scanning electronic microscope (SEM) [19-21] or backscattered electrons (BSE) [22, 23] observation is complex and time-consuming, and thus difficult to measure the thickness and distribution of the rust layer and conduct parametric study. Even though many different models for non-uniform corrosion have been proposed, they do not specify the realistic positions of the peaks of reinforcement corrosion and can only be applied to the simplest one-peak distribution, which can oversimplify the accurate situation in real corroded reinforced concrete structures involving multiple peaks. With the exception of some limited experimental data, there is currently no method available or reported even for a preliminary prediction of the parameters to determine the non-uniform corrosion of reinforcements.

This study therefore proposes an analogous method based on minimizing the Wasserstein distance (WD) to predict the distribution of the non-uniform corrosion on reinforcements. The WD is a distance function defined between two distributions that are not known on a given metric space, which can be visualized as the cost of turning one distribution into the other [24, 25]. The WD is thus used in this study to compare the base distribution and target predicted distribution. Compared to the existing models of non-uniform corrosion of reinforcement, the proposed WD-based analogous method utilized the relationships between the distribution of rust and the positions of concrete cracks observed in the tests [20, 21]. This can overcome the aforementioned limitations of the existing models as the crack pattern of concrete induced by reinforcement corrosion can be easily observed without using SEM or BSE.

The method is validated through all of the available experimental results [19-21] that can be found in the literature to the best of our knowledge. The non-uniformity and the total area of the rust layer, characterizing the environment of corrosion and confinement of concrete, are selected as the key parameters for determining the distribution of non-uniform corrosion on reinforcements. Empirical equations of the non-uniformity and the total area of the rust layer are expressed as a function of the degree of corrosion. The distribution of corrosion at different degrees of corrosion can thus be predicted by inputting different values of the non-uniformity and the total area of rust. The method presented in this study addresses the research gap and quantifies the distribution of non-uniform corrosion on reinforcements by realistically simulating the propagation of cracking in concrete.

2. State-of-the-art models for non-uniform corrosion of reinforcement

Steel rebars are usually embedded in a non-uniform concrete cover to protect them against corrosion and other damage; see Figure 1a. However, chloride ions can diffuse into the steel surface through the concrete and initiate local corrosion. Active corrosion occurs at the tip of crack or the surrounding areas of the damaged interface between the concrete and steel, because the shortest path for the chloride ions to penetrate the rebar is provided. Cathodic reactions take place on the passive steel surfaces. An electrochemical process then takes place, which is similar to a galvanic reaction due to electrical contact between the active steel and the surrounding passive steel [26]; see Figure 1b. In the cross section I-I (Figures 1c and 1d) of the active area (Figure 1b), the active steel zone is facing the side of the concrete cover which is thinner. The passive steel area is further away from the concrete cover. As a result, rust is distributed in the active area where the cover is thinner. This non-uniform distribution of rust causes higher tensile pressure and reduces the service life of structures, compared to uniformly distributed rust. Therefore, it is imperative to determine the non-uniform distribution of localized reinforcement corrosion by simulating the stress field and the cracking propagation process of concrete.

Many different models on the non-uniform corrosion of reinforcement can be found in the literature. The distribution of rust around the reinforcement from different models is shown in Figure 2. The changes in the thickness of the rust layer (T_{CL}) versus the theta angle in the different models are illustrated in Figure 3. In these models, the rust is prescribed to distribute over an angle θ from 0 to 2π. The maximum thickness of the rust layer ($T_{CL}^{\max}$) is specified as the π angle. Most of the models show a one-peak distribution, while Zhao et al. [21] present both one-peak and multi-peak distributions (see Figure 4).

Though the pitting corrosion of reinforcement generally shows a hollowing shape, it is found that many models [10-21] used single peak smooth curves to simulate the distribution of rust on reinforcement. This is because the evolution of concrete cracks is significantly affected by the peaks of the distribution of rust. It is unnecessary and difficult to accurately model the entire distribution of rust surrounding the reinforcement. Zhao et al. [21] found that the number of peaks of the rust distribution corresponds to the number of concrete cracks. The positions of peaks normally near the inner end of the concrete cracks.

The presence of corrosion-induced concrete cracks is the main reason for the peaks of rust distribution. When a crack has not been formed or there is only one crack in concrete, the distribution of rust can be fitted as a one-peak distribution, which is generally a smooth distribution. However, when there is more than one crack in concrete, the distribution of rust is usually modeled by a multi-peak distribution with a hollow hole surrounding the reinforcement as shown in Figure 4.

None of the aforementioned models have identified the changes in the distribution of non-uniform corrosion versus the degree of corrosion. Although the shape of the distribution of corrosion products has been well modelled, the value of the parameters in the proposed models with different degrees of corrosion has not been specified. Therefore, a method that can determine the distribution of non-uniform corrosion on reinforcements is very much needed.

3. Method to determine distribution of non-uniform corrosion

In this section, an analogous method to determine the distribution of non-uniform corrosion on reinforcements will be discussed. The use of analogy is a basic comparison method of two methods that have the same principle but used in different fields or to solve different issues. In the *Dictionary of Philosophy of Mind*, analogy is described as “a systematic comparison between structures that uses properties of and relations between objects of a source structure to infer properties of and relations between objects of a target structure” [27]. Analogous methods have been widely utilized in the field of artificial intelligence, such as curve analogies [28] and image analogies [29]. In this study, we explore the use of analogy as a means to predict the non-uniform distribution of corrosion on reinforcements.

The problem can be described as shown in Figure 5: given that there is a known non-uniform distribution of corrosion $F_B(\theta)$ (base distribution), a new distribution $F_T(\theta)$ (target distribution) needs to be predicted with characteristic parameters including the non-uniformity R_p and the total area of the rust layer A_{CL}.

This can be mathematically illustrated as a process to move the points P_i of weight $w(\theta)$ on $F_B(\theta)$ to points P'_i on $F_T(\theta)$. The work or energy is well known as the WD. This study pursues to find $F_T(\theta)$ with minimum WD as the most analogous distribution of $F_B(\theta)$ constrained by the given R_p and A_{CL}. The method is based on the analogy between $F_B(\theta)$ and $F_T(\theta)$.

As previous studies [18, 20, 21] have found that the Gaussian model has good accuracy in fitting experimental data. In addition, both one-peak and multi-peak distributions of non-uniform reinforcement corrosion can be modelled by Gaussian functions. Thus, the proposed analogous method is based on a Gaussian model for the non-uniform corrosion of reinforcements as:

$$T_{CL} = \sum_i H_i e^{-\left(\frac{\theta - pos_i}{\sqrt{2}\sigma_i}\right)^2} \tag{1}$$

where H_i and σ_i are the height of the peak and standard variance of i^{th} sub-Gaussian function at peak position pos_i, respectively.

As aforementioned, the number of peaks in the fitted Gaussian function in Eq. (1) corresponds to the number of concrete cracks. The peak positions of the fitted Gaussian function normally near the inner end of concrete cracks [21]. In conclusion, the distribution of T_{CL} is highly dependent on the crack pattern, which differs with the geometry and mechanical properties of specimens, as well as the environment of corrosion. Nevertheless, for specimens under the same boundary condition and environment of corrosion, the crack pattern is similar at different degrees of corrosion. As a result, the distribution of T_{CL} is similar at different degrees of corrosion for specimens with the same conditions and can be applied to analogy purposes.

3.1. Non-uniformity and total area of rust layer

The non-uniformity of corrosion on reinforcements can be quantified by using the pitting corrosion factor R_p, which was first proposed by Gonzalez et al. [9], as

$$R_p = \frac{p_{\max}}{p_{av}} \tag{2}$$

where $p_{\max}$ is the maximum depth of the corrosion, and p_{av} is the average depth of the corrosion. R_p has been widely adopted to describe the non-uniformity of rebar corrosion [30]. In this study, the corrosion depth is quantified with T_{CL}, and thus Eq. (2) can be modified as:

$$R_p = \frac{T_{CL}^{\max}}{A_{CL}/(\pi D)} \tag{3}$$

where $T_{CL}^{\max}$ is the maximum thickness of the rust layer around the circumference of a corroded rebar, and A_{CL} is the total area of the rust layer.

Gu et al. [30] argued that the pitting corrosion factor R_p should take the complex geometry of pits and their random distribution into consider, and used the spatial variability factor R_{sp} to quantify the non-uniformity of corrosion between different cross sections along a corroded rebar. However, in the present study, R_{sp} is not considered because R_{sp} = 1 when investigating the distribution of rust surrounding the circumference of reinforcement.

As shown in Figure 4, the A_{CL} is obtained by integrating T_{CL} over θ from 0 to 2π, i.e.,

$$A_{CL} = \int_0^{2\pi} T_{CL}\left(D/2\right) d_\theta \tag{4}$$

where D is the rebar diameter.

Substituting Eq. (1) into Eq. (4), the total area of rust layer A_{CL} can be evaluated as:

$$A_{CL} = \int_0^{2\pi} T_{CL}\left(D/2\right) d_\theta = \int_0^{2\pi} \sum_i H_i e^{-\left(\frac{\theta - pos_i}{\sqrt{2}\sigma_i}\right)^2} \left(D/2\right) d_\theta \tag{5}$$

It is found from Eq. (5) that the A_{CL} depends on the height of the peak H and standard variance σ. Thus, A_{CL} can be an alternative parameter of H or σ to characterize the shape of the Gaussian function. In addition, $T_{CL}^{\max} = \max(H_i)$ can be determined by R_p and A_{CL} with Eq. (3), which means that the non-uniformity R_p and the A_{CL} can be applied as two independent parameters to characterize the Gaussian function of the non-uniform corrosion. A_{CL} describes the total amount of steel corrosion, while R_p characterize the non-uniformity of the corrosion of the rebar.

3.2. Analogous method for non-uniform corrosion of reinforcement

The Gaussian model will be used to demonstrate the proposed analogous method. The non-uniformity R_p and the total area of rust A_{CL} are used as the two parameters that characterize the Gaussian function (see Section 3.1). The analogous characteristics of the Gaussian function-based non-uniform corrosion of the reinforcement can be summarized as:

(1) analogous Gaussian functions. Three independent parameters, i.e. non-uniformity,

the total area, and the peak position can be used to determine a one-peak Gaussian function;

(2) analogous non-uniform corrosion of the reinforcement. The number of Gaussian peaks corresponds to the number of concrete cracks. The peak positions of the Gaussian function correspond to the crack directions; and

(3) analogous non-uniform corrosion of the reinforcement at different degrees of corrosion. The distribution of T_{CL} is very dependent on the crack pattern, which is similar at different degrees of corrosion for specimens subjected to the same confinement of concrete and environment of corrosion. Therefore, the distribution of T_{CL} is analogous at different degrees of corrosion among specimens with the same parameters and under the same environment of corrosion.

Based on these analogous characteristics, the $F_T(\theta)$ is determined to be the most analogous distribution of the $F_B(\theta)$ among all of the possible distributions with a given R_p and A_{CL}, which is mathematically expressed as:

$$E = \min \frac{\sum_{\theta} w(\theta)\sqrt{\left|F_B(\theta)-F_T(\theta)\right|^2}}{\sum_{\theta} w(\theta)} \tag{6}$$

subject to

$$A_{CL} = \int_0^{2\pi} T_{CL}\left(D/2\right)d_{\theta} \tag{7a}$$

$$R_p = \frac{T_{CL}^{\max}}{A_{CL}/\left(\pi D\right)} \tag{7b}$$

$$\frac{A_{CL}}{A_0} = \left(1-\frac{1}{R_{sp}}\right)+\frac{1}{R_{sp}}\frac{A_{CL}}{A_0} \tag{7c}$$

where $w(\theta)$ is the weight function of $F_B(\theta)$.

When the weight function $w(\theta)$ is considered to be the weight of points of

$F_B(\theta)$, Eq. (6) provides a value that has a physical meaning which shows that $F_B(\theta)$ is the minimum work needed to create the most analogous $F_T(\theta)$ (see Figure 5). This is well known as the earth mover's distance (EMD) in statistics [24] or WD in mathematics [25]. Therefore, the proposed method is called the WD-based analogous method here. For the problem in this study, $w(\theta)$ is chosen as a constant of one unit, i.e. $w(\theta)=1$. Therefore, Eq. (6) is equivalent to

$$E = \min \left\| F_B(\theta) - F_T(\theta) \right\|^2 \tag{8}$$

Specifically, when applying the WD-based analogous method to predict the non-uniform corrosion of reinforcements, the following assumptions can be made based on the analogous characteristics such as the convergence acceleration of the minimization process of Eq. (8), i.e.,

(a) the peak positions of $F_T(\theta)$ are the same as those of $F_B(\theta)$. This is because the WD-based method is based on the analogy between $F_B(\theta)$ and $F_T(\theta)$. However, in cases of one-peak Gaussian distributions whose peak position is prescribed as $\theta = \pi$, this has been met automatically; and

(b) both $F_B(\theta)$ and $F_T(\theta)$ are modelled as Gaussian functions. The latter can be achieved by finding appropriate modification factors of the height of peaks H_i and standard variances σ_i of $F_B(\theta)$.

Based on these assumptions, for a given $F_B(\theta)$:

$$F_B(\theta) = \sum_i H_i e^{-\left(\frac{\theta - pos_i}{\sqrt{2}\sigma_i}\right)^2} + \Delta_1 \tag{9a}$$

$F_T(\theta)$ is assumed to be

$$F_T(\theta) = \sum_i (\lambda_i H_i) e^{-\left(\frac{\theta - pos_i}{\sqrt{2}(\sigma_i / k_i)}\right)^2} + \Delta_2 \tag{9b}$$

where Δ_1 and Δ_2 are the minimum T_{CL} around the circumference of the corroded reinforcement which might be non-zero in the distributions of some samples (R-3, R-5 and R-19 in Zhao et al. [20] for instance). H_i, σ_i and Δ_1 are known parameters. λ_i and k_i are modified factors of the i^{th} peak height H_i and i^{th} standard variance σ_i, respectively. It is noted that λ_i, k_i, Δ_1 and Δ_2 are nonnegative.

Substituting Eq. (9) into Eq. (8) gives

$$E = \min_{\lambda_i, k_i, \Delta_2} \left\| \sum_i H_i e^{-\left(\frac{\theta - pos_i}{\sqrt{2}\sigma_i}\right)^2} - \sum_i \left(\lambda_i H_i\right) e^{-\left(\frac{\theta - pos_i}{\sqrt{2}(\sigma_i / k_i)}\right)^2} + \left(\Delta_1 - \Delta_2\right) \right\|^2 \tag{10}$$

subject to Eq. (7) and λ_i, k_i, $\Delta_i > 0$.

$F_T(\theta)$ can be determined by solving Eq. (10) and obtaining λ_i, k_i and Δ_2. In this study, the constrained single-objective minimization problem is implemented using a built-in function in MATLAB.

4. Validation of proposed method

4.1. Experiments of Yuan and Ji [19] and Zhao et al. [20, 21]

The experimental results in Yuan and Ji [19] and Zhao et al. [20, 21] are used in this study to demonstrate and validate the proposed method. Yuan and Ji [19] examined specimens that were deteriorated under a laboratory environment of 35 °C at a relative humidity of 90%. The designed cubic compressive strength of concrete was 20 MPa. The dimensions of the specimens were 200 mm × 150 mm× 63 mm. A single damaged reinforcement was placed onto the corner of the tested specimen. The thinnest cover was 30 mm. Cylinder shaped specimens were cut from the tested specimens with different corrosion levels and prepared so that they could be observed under an SEM.

Zhao et al. [20] subjected concrete specimens to cyclic wetting and drying in environmental chamber for about 2 years. Each cycle of testing lasted for 3 days.

They used 3.5 wt. % sodium chloride solution to mist the specimens for 4 hours and dried them at 40 °C until next cycle. The concrete was mixed with slag and fly ash. The water binder ratio was 0.345. Portland cement CEM I 42.5N (EN197-1:2000) was used for the cast of concrete. The 28-day compressive strength of concrete cube was 56 MPa. The size of the specimens was 150 mm × 150 mm× 300 mm. Three deformed carbon steel rebars with a diameter of 16 mm were casted into each concrete specimen and faced the top of the specimen. The cover thickness was 20 mm. Two steel rebars were placed on the left corner (labelled L) or right corner (labelled R), while the third steel rebar was placed in the middle (labelled M). The corroded specimens were cut and polished to observe the T_{CL} around the circumference of the reinforcement under an SEM.

Zhao et al. [21] adopted a similar methodology as that of Zhao et al. [20] to observe the distribution of rust surrounding the reinforcement, apart from different exposure history and mix properties of concrete specimen. Two specimens were prepared and subjected to 3.5-5 wt. % sodium chloride solution or mist under cyclic wetting and drying environment. The water-to-binder ratios of Specimens TC30 and AC40 were, respectively, 0.56 and 0.44, with no mixture of slag and fly ash. The 28-day compressive strengths of concrete cubes of Specimens TC30 and AC40 were 38.2 MPa and 49.9 MPa, respectively.

4.2. Validation of analogy of Gaussian distribution

The proposed WD-based analogous method can be used to predict non-uniform corrosion with a comparison of the distribution of different specimens. As the multi-peak distribution of rust is rarely reported in the literature except the one given by Zhao et al. [21], validation of the WD-based analogous method in the present study will only focus on the one-peak distribution of rust.

It is noted that $F_B(\theta)$ should have the same peak positions as those of $F_T(\theta)$, which intrinsically indicates the corroded specimen of $F_B(\theta)$ has the same crack pattern as that of $F_T(\theta)$. As discussed in Zhao et al. [20], the distribution of rust for specimens of Yuan and Ji [19] and Zhao et al. [20, 21] can be modelled with a one-peak Gaussian function, in which the peak position is prescribed as $\theta = \pi$. As a consequence, this requirement has been met automatically.

As the peak positions are all the same, the base distribution $F_B(\theta)$ can thus be randomly selected as the distribution of sample R-15 of Zhao et al. [20] which reads:

$$F_B\left(\theta\right) = 0.1432e^{-\left(\frac{\theta-\pi}{\sqrt{2}\times 1.325}\right)^2} \tag{11}$$

where the minimum thickness of rust $\Delta_1 = 0$.

The target distribution $F_T\left(\theta\right)$ of other samples to be predicted is assumed to be:

$$F_T\left(\theta\right) = He^{-\left(\frac{\theta-pos_i}{\sqrt{2}\sigma}\right)^2} + \Delta_2 \tag{12}$$

where $H = 0.1432\lambda$, $\sigma = 1.325/k$, in which λ, k and Δ_2 are parameters to be calculated by solving Eq. (10).

Figure 6 shows the predicted $F_T(\theta)$ of samples R-3, R-5, and M-15 of Zhao et al. [20] and CorExp-B6 of Yuan and Ji [19]. It can be observed that the predicted results with the use of the proposed analogous method are in close agreement with the fitted results of Zhao et al. [20]. The predicted results have a close goodness of fit with the results in Zhao et al. [20]. The goodness of fit is assessed with R^2 as:

$$R^2 = 1 - \frac{\sum_i \left(y_i - \hat{y}_i\right)^2}{\sum_i \left(y_i - \bar{y}_i\right)^2} \tag{13}$$

As shown in Figure 6, the maximum values of the predicted results equal the maximum values of the experimental results, whilst the maximum values of the fitted results of Zhao et al. [20] are slightly less than the maximum values of the experimental results. This is because the predicted results based on the WD-based analogous method are limited by Eq. (7b). As a result, the predicted results are heavily dependent on the fit of the given R_p and $A_{av,\,CL}$. This can be further illustrated in Figure 7, which shows the predicted $F_T(\theta)$ of samples R-14 and R-19 of Zhao et al. [20]. As can be observed in Figure 7a, the point of the maximum value of the experimental T_{CL} is scattered with others. When R_p is obtained using this point, the predicted distribution $F_T^1(\theta)$ has a goodness of fit of R^2 = 0.76. Alternatively, when R_p is obtained using the maximum fitted value of Zhao et al. [20], the goodness of fit of the predicted distribution $F_T^2(\theta)$ is R^2 = 0.896 (which is the same as that in Zhao et al. [20]). This is also the same for the predicted result of sample R-19 in Figure 7b.

The distributions of the remaining specimens of Zhao et al. [20] are used to validate the proposed model, see Table 1. It is noted that R^2 is obtained by comparing the predicted distribution with the results calculated with H, σ and Δ_2 fitted through experimental results. It is observed that R^2 are generally larger than 0.93 except $R^2 = 0.86$ of sample R-2.

The predicted parameters H, σ and Δ_2 for samples of specimens TC30 and AC40 of Zhao et al. [21] are compared with the values fitted by experimental data as shown in Table 2 and Table 3, respectively. It is found that R^2 of the predicted distributions of specimen TC30 are always larger than 0.88. The WD-based analogous method shows a better performance for the prediction of specimen TC30 than that of specimen AC40. As shown in Table 3, the R^2 of the predicted distributions of specimen AC40 are generally larger than 0.9, whilst R^2 of three samples are less than 0.6. The height of peak H of specimen AC40 is much larger than that of specimen TC30, which indicates that the corrosion of specimen AC40 is less severe than specimen TC30. As the thickness of rust of some samples of specimen AC40 is very small, it is difficult to be accurately predicted because even a minor absolute error can cause a large discrepancy.

It is noted that all the available experimental data that can be found in the literature has been used to validate the proposed model. To further valid the proposed method, more experiments should be performed to obtain the distribution of rust surrounding the circumference of reinforcement.

5. Application of WD-based analogous method to practical case

$F_B(\theta)$ and the characteristic parameters, i.e. R_p and A_{CL}, of $F_T(\theta)$ should be obtained to apply the proposed WD-based analogous method to a practical case. $F_B(\theta)$ is required to have the same peak positions as those of $F_T(\theta)$. As discussed in Section 2, few related studies on multi-peak Gaussian distributions have been reported. Therefore, this section will focus on the use of a one-peak Gaussian distribution based on the experimental results in a laboratory environment [20].

As shown in Table 4, the data on $T_{CL}^{\max}$ and A_{CL} versus the degree of corrosion ρ for the weight loss are adapted from Zhao et al. [20]. As discussed in Section 4.2, it is best to select $T_{CL}^{\max}$ and A_{CL} from the fitted Gaussian function which has the best fit to all of the experimental data. The corresponding R_p (non-uniformity) is calculated with Eq. (3).

Figures 8-10 show the variations in the A_{CL}, $T_{CL}^{\max}$ and R_p with degree of corrosion ρ (wt. %). It can be observed from Figure 8 that A_{CL} is linearly proportional to ρ. The fitted A_{CL} with a goodness of fit $R^2 = 0.9732$ is expressed as:

$$A_{CL} = 3.6888\rho \quad (14)$$

The $T_{CL}^{\max}$ is scattered between a lower bound of $T_{CL}^{\max} = 0.101\rho$ and an upper bound of $T_{CL}^{\max} = 0.491\rho$ as shown in Figure 9. The best fitted curve of $T_{CL}^{\max}$ is a quadratic function of ρ ($R^2 = 0.72$), which is

$$T_{CL}^{\max} = 0.2568\rho - 0.0174\rho^2 \tag{15}$$

As $T_{CL}^{\max}$ is between 0.101ρ and 0.491ρ, the R_p (non-uniformity) ranges from 1.38 to 6.69 based on Eqs. (3) and (14). This observation of the R_p is similar to that of Gonzalez et al. [9] which varies from 2.7 to 5.3.

As evident in Figure 10, the curve of R_p calculated by using Eqs. (14) and (15) is expressed as:

$$R_p = 3.499 - 0.237\rho, \tag{16}$$

which passes through the lower bound,

$$R_p = \begin{cases} 2.138 - 0.2321\rho & \rho \le 2.78 \\ 1.493 & \rho > 2.78 \end{cases} \tag{17}$$

and the upper bound.

$$R_p = \begin{cases} 6.465 - 1.191\rho & \rho \le 2.78 \\ 3.154 & \rho > 2.78 \end{cases} \tag{18}$$

6. Conclusion

An analogous method is proposed based on minimizing the WD to predict the non-uniform corrosion of reinforcements. The analogous characteristics of the distribution of non-uniform corrosion on reinforcements are summarized from the corresponding relationships between the distribution of rust and the crack pattern of concrete observed in previous experiments. This enables the WD-based analogous method to predict the distribution of rust for samples with similar crack patterns.

The method is found to have good performance in predicting the Gaussian distributions of non-uniform corrosion. The non-uniformity R_p and the A_{CL} are selected as the inputted characteristic parameters. To apply the WD-based method in practical projects, the relationship between the input parameters R_p and A_{CL} are fitted based on the experimental results in a laboratory environment. Therefore, the following conclusions are made based on the observations in this study:

(1) the distributions of the non-uniform corrosion of reinforcements are analogous at different degrees of corrosion in samples with similar crack patterns. The distributions modelled by Gaussian functions are analogous. These are the basis of the WD-based analogous method for prediction purposes.

(2) The non-uniform corrosion at different degrees of corrosion has been proven to be well predicted. The R_p and A_{CL} are fitted as functions of the degree of corrosion ρ. Thus, the distribution of the non-uniform corrosion at different ρ can be predicted.

(3) The input parameters can affect the accuracy of the predicted results. The R_p and A_{CL} obtained from the best fitting results can improve the overall prediction accuracy. For actual engineering projects, the average of several of the highest T_{CL} values is recommended for calculating R_p.

(4) More research work especially experiments should be carried out on the multi-peak Gaussian distribution of non-uniform corrosion on reinforcements and the estimation of the non-uniformity and the total area of rust.

7. Acknowledgement

The authors would like to thank Dr. Liu Yongliang of Jilin University for his invaluable advice while preparing the manuscript.

References:

[1] C. Andrade, C. Alonso, F.J. Molina, Cover cracking as a function of rebar corrosion: Part 1 – experimental test, Mater. Struct. 26 (9) (1993) 453–464.

[2] C. Alonso, C. Andrade, J. Rodriguez, J. M. Diez, Factors controlling cracking of concrete affected by reinforcement corrosion, Mater. Struct. 31 (7) (1998) 435–441.

[3] Y.P. Liu, R.E. Weyers, Modeling the time-to-corrosion cracking in chloride contaminated reinforced concrete structures, ACI Mater. J. 95 (1998) 675–681.

[4] S.J. Pantazopoulou, K.D. Papoulia, Modeling cover cracking due to reinforcement corrosion in RC structures, ASCE J. Eng. Mech. 127 (4) (2001) 342-351.

[5] K. Bhargava, A.K. Ghosh, Y. Mori, S. Ramanujam, Model for cover cracking due to rebar corrosion in RC structures, Eng. Struct. 28 (8) (2006) 1093-1109.

[6] T. El Maaddawy, K. Soudki, A model for prediction of time from corrosion initiation to corrosion cracking, Cem. Concr. Comps. 29 (3) (2007) 168-175.

[7] L. Chernin, Leon, V. Val. Dimitri, Prediction of corrosion-induced cover cracking in reinforced concrete structures, Constr. Build. Mater. 25 (4) (2011) 1854-1869.

[8] Q. F. Liu, R. K. L. Su, A displacement-based inverse analysis method to estimate in-situ Young's modulus of steel rust in reinforced concrete, Eng. Frac. Mech. 192 (2018) 114-128.

[9] J. A. Gonzalez, C. Andrade, C. Alonso, S. Feliu, Comparison of rates of general corrosion and maximum pitting penetration on concrete embedded steel reinforcement, Cem. Concr. Res. 25 (2) (1995) 257-264.

[10] B. S. Jang, B. H. Oh, Effects of non-uniform corrosion on the cracking and service life of reinforced concrete structures, Cem. Concr. Res. 40 (9) (2010) 1441-1450.

[11] B. Šavija, M. Luković, J. Pacheco, E. Schlangen, Cracking of the concrete cover due to reinforcement corrosion: a two-dimensional lattice model study, Constr. Build. Mater. 44 (2013) 626-638.

[12] A. Chen, Z. Pan, R. Ma, Mesoscopic simulation of steel rebar corrosion process in concrete and its damage to concrete cover, Str. Infra. Eng. 13 (4) (2017) 478-493.

[13] T. Pan, L. Yang, Stochastic modeling of reinforced concrete cracking due to nonuniform corrosion: FEM-based cross-scale analysis, J. Mater. Civ. Eng. 24 (6) (2011) 698-706.

[14] K. K. Tran, H. Nakamura, K. Kawamura, M. Kunieda, Analysis of crack propagation due to rebar corrosion using RBSM, Cem. Concr. Comps. 33 (9) (2011) 906-917.

[15] D. Qiao, H. Nakamura, Y. Yamamoto, T. Miura, Crack patterns of concrete with a single rebar subjected to non-uniform and localized corrosion, Constr. Build. Mater. 116 (2016) 366-377.

[16] J. Zhang, X. Ling, Z. Guan, Finite element modeling of concrete cover crack propagation due to non-uniform corrosion of reinforcement, Constr. Build. Mater. 132 (2017): 487-499.

[17] C. Zhen, A. Alipour, Concrete cover cracking and service life prediction of reinforced concrete structures in corrosive environments, Constr. Build. Mater. 159 (2018) 652-671.

[18] X. Xun, S. Yang, C. Q. Li, A non-uniform corrosion model and meso-scale fracture modelling of concrete, Cem. Concr. Res. 108 (2018) 87-102.

[19] Y. Yuan, Y. Ji, Modeling corroded section configuration of steel bar in concrete structure, Constr. Build. Mater. 23 (6) (2009) 2461-2466.

[20] Y. Zhao, B. Hu, J. Yu, W. Jin, Non-uniform distribution of rust layer around

steel bar in concrete, Corros. Sci. 53 (12) (2011) 4300-4308.

[21] Y. Zhao, Non-uniform distribution of a corrosion layer at a steel/concrete interface described by a Gaussian model, Corros. Sci. 112 (2016) 1-12.

[22] F. Chen, C. Q. Li, H. Baji, B. Ma, Effect of design parameters on microstructure of steel-concrete interface in reinforced concrete, Cem. Concr. Res. 119 (2019) 1-10.

[23] F. Chen, C. Q. Li, H. Baji, B. Ma, Quantification of steel-concrete interface in reinforced concrete using Backscattered Electron imaging technique. Constr. Build. Mater. 179 (2018) 420-429.

[24] Y. Rubner, T. Carlo, J. G. Leonidas, The earth mover's distance as a metric for image retrieval, Int. J. Comp. Vision 40 (2) (2000): 99-121.

[25] V. Cédric, The Wasserstein distances, Optimal Transport, Springer, 2009.

[26] R. Francois, L. Stéphane, D. Fabrice, Corrosion and Its Consequences for Reinforced Concrete Structures, Elsevier, 2018.

[27] C. Eliasmith, Dictionary of Philosophy of Mind, https://sites.google.com/site/minddict/analogy.

[28] A. Hertzmann, N. Oliver, B. Curless, S. M. Seitz, Curve Analogies, In Rendering Techniques (2002) 233-246.

[29] A. Hertzmann, C. E. Jacobs, N. Oliver, B. Curless, D. H. Salesin, Image analogies, In Proceedings of the 28th annual conference on Computer graphics and interactive techniques. ACM, 2001.

[30] X. Gu, H. Guo, B. Zhou, W. Zhang, C. Jiang, Corrosion non-uniformity of steel bars and reliability of corroded RC beams, Eng. Str.167 (2018) 188-202.

Table 1. Verification for samples of Zhao et al. [20].

Sample	H		σ		Δ_2		R^2
	Exp	Pred	Exp	Pred	Exp	Pred	
R-1	0.26	0.2404	0.6477	0.4969	0.3523	0.3718	0.948
R-2	0.5809	0.6417	0.4441	0.6394	0.4059	0.3451	0.861
R-4	0.8589	0.8708	0.4256	0.4541	0.2028	0.1909	0.996
R-7	0.1274	0.1205	0.4783	0.3611	0.0114	0.0184	0.943
R-8	0.3638	0.367	0.384	0.4027	0.0042	0.001	0.998
R-9	0.4492	0.4399	0.1734	0.1236	0.0133	0.0227	0.926
R-17	0.125	0.1195	1.0467	0.9788	0.0256	0.0311	0.997
R-18	0.2582	0.2578	0.7215	0.7189	0.0528	0.0532	0.999

Table 2. Verification for samples of specimen TC30 of Zhao et al. [21].

Sample	H		σ		Δ_2		R^2
	Exp	Pred	Exp	Pred	Exp	Pred	
TC30 R1	0.7952	0.8042	0.742	0.7618	0.042	0.033	0.999
TC30 R3	0.6713	0.656	0.766	0.7254	0.104	0.1193	0.997
TC30 R4	0.5452	0.5592	0.641	0.6877	0.015	0.001	0.995
TC30 R7	0.469	0.4905	0.245	0.3444	0.175	0.1534	**0.888**
TC30 L5	0.4826	0.4757	0.763	0.7375	0.058	0.0649	0.999
TC30 M6	0.4859	0.4632	0.803	0.7193	0.072	0.0947	0.99
TC30 M13	0.422	0.3479	0.964	0.6302	0.128	0.203	**0.882**
TC30 R5	0.4667	0.465	0.712	0.7051	0	0.0018	0.999
TC30 R6	0.6005	0.5711	0.845	0.7593	0	0.0294	0.991
TC30 R8	0.3997	0.3987	0.533	0.5281	0	0	0.99
TC30 R9	0.4957	0.4947	0.627	0.6232	0	0	0.99
TC30 R10	0.4643	0.4554	0.8	0.7668	0	0.0089	0.998
TC30 R11	0.3116	0.2849	0.9	0.7487	0	0.0268	0.974
TC30 R12	0.6292	0.6282	0.48	0.4768	0	0	0.999
TC30 R13	0.4021	0.3689	1.018	0.8818	0	0.0332	0.985
TC30 R14	0.3565	0.3555	0.677	0.6719	0	0	0.999
TC30 R15	0.3839	0.3224	1.011	0.7229	0	0.0616	0.924
TC30 R16	0.5479	0.5469	0.573	0.5695	0	0.0222	0.986
TC30 L6	0.7358	0.7348	0.617	0.6144	0	0	0.999
TC30 L10	0.3483	0.3317	0.843	0.7596	0	0.0166	0.991
TC30 M3	0.4075	0.4065	0.702	0.6976	0	0	0.999
TC30 M10	0.6039	0.6029	0.615	0.6119	0	0	0.999

Table 3. Verification for samples of specimen AC40 of Zhao et al. [21].

Sample	H		σ		Δ_2		R^2
	Exp	Pred	Exp	Pred	Exp	Pred	
AC40 M2	0.024	0.0281	0.716	0.9811	0.012	0.0078	0.902
AC40 M5	0.0144	0.016	0.805	0.9802	0.006	0.0044	0.964
AC40 M7	0.0198	0.0209	0.222	0.345	0.005	0.0039	0.805
AC40 R1	0.0313	0.033	0.14	0.1806	0.005	0.0034	0.9
AC40 R2	0.0327	0.033	0.183	0.2046	0.004	0.0037	0.989
AC40 R4	0.01308	0.0138	0.122	0.2402	0.003	0.0023	**0.519**
AC40 M8	0.0209	0.0199	0.61	0.5148	0	0	0.977
AC40 M9	0.0149	0.0139	0.561	0.4214	0	0	0.94
AC40 M10	0.0242	0.0232	0.89	0.8203	0	0	0.995
AC40 M11	0.0273	0.026	1.022	0.9466	0	0.0013	0.996
AC40 M12	0.0095	0.0075	0.794	0.3368	0	0.002	0.647
AC40 M13	0.0108	0.0083	1.333	0.9835	0	0.0025	0.944
AC40 M14	0.0159	0.01487	0.905	0.7973	0	0	0.987
AC40 M16	0.0061	0.0051	1.109	0.8358	0	0	0.947
AC40 M17	0.008	0.0063	0.75	0.2768	0	0.001693	**0.575**
AC40 M18	0.0069	0.0051	0.928	0.38	0	0.001773	0.628
AC40 R6	0.0152	0.01371	1.105	0.9562	0	0.001455	0.985
AC40 R8	0.0092	0.0072	1.304	0.98	0	0.001948	0.95
AC40 R11	0.0056	0.004	0.929	0.3312	0	0.001534	**0.556**

Table 4. Maximum thickness of rust layer and total area of rust layer of samples adapted from Zhao et al. [20].

Sample	T_{CL}^{max} (mm)	A_{CL} (mm^2)	R_p	Degree of corrosion (wt. %)
R-1	0.612	21.085	1.460	6.07
R-3	1.102	22.349	2.479	5.89
R-4	1.062	17.525	3.045	4.71
R-5	0.854	12.884	3.334	3.5
R-6	0.212	4.845	2.198	1.16
R-7	0.139	1.795	3.888	0.55
R-8	0.368	3.014	6.137	0.75
R-10	0.605	9.359	3.249	2.34
R-11	0.485	9.734	2.505	2.78
R-12	0.513	7.535	3.425	2.2
R-13	0.280	2.370	5.944	0.64
R-14	0.139	3.986	1.755	0.53
R-15	0.241	2.897	4.185	0.76
R-16	0.141	4.282	1.651	1.06
R-17	0.151	3.910	1.936	1.13
R-18	0.311	6.390	2.447	1.96
R-19	0.238	5.658	2.114	1.63
R-20	0.265	10.320	1.289	2.61

Notes: θ = direction, A_{CL} = total area of rust layer and R_p = pitting corrosion factor

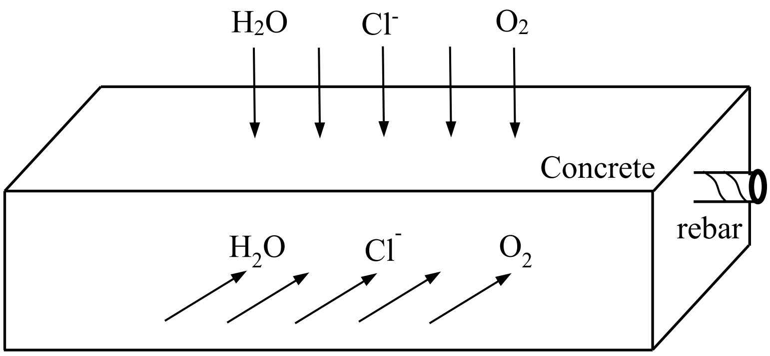

(a) Rebar in concrete with non-uniform cover thickness.

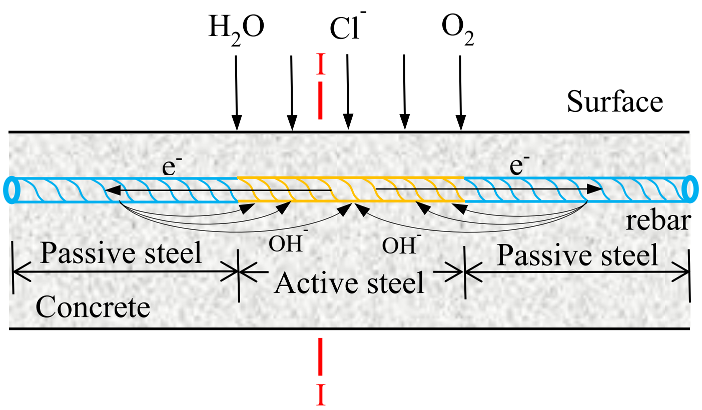

(b) Galvanic reaction formed between active steel and surrounding passive steel.

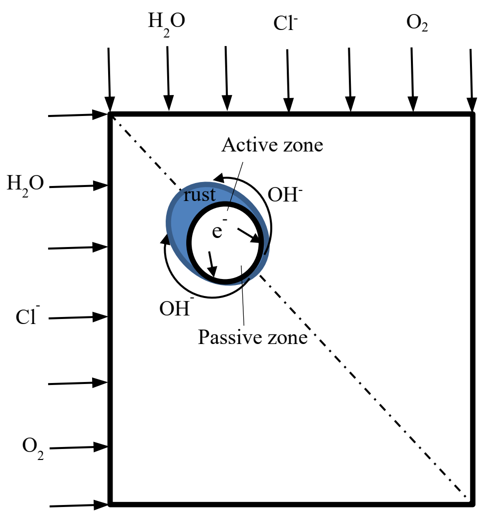

(c) Localized corrosion of rebar in corner of concrete.

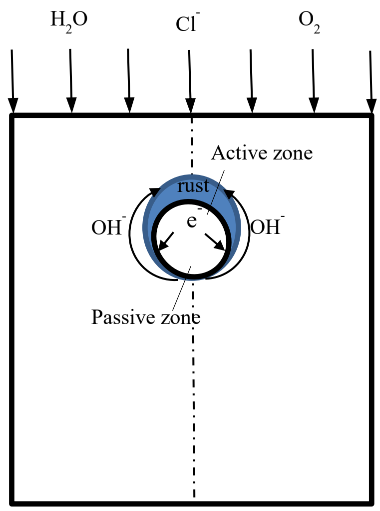

(d) Localized corrosion of rebar facing top surface of concrete.

Figure 1. Illustration of localized corrosion induced by chloride.

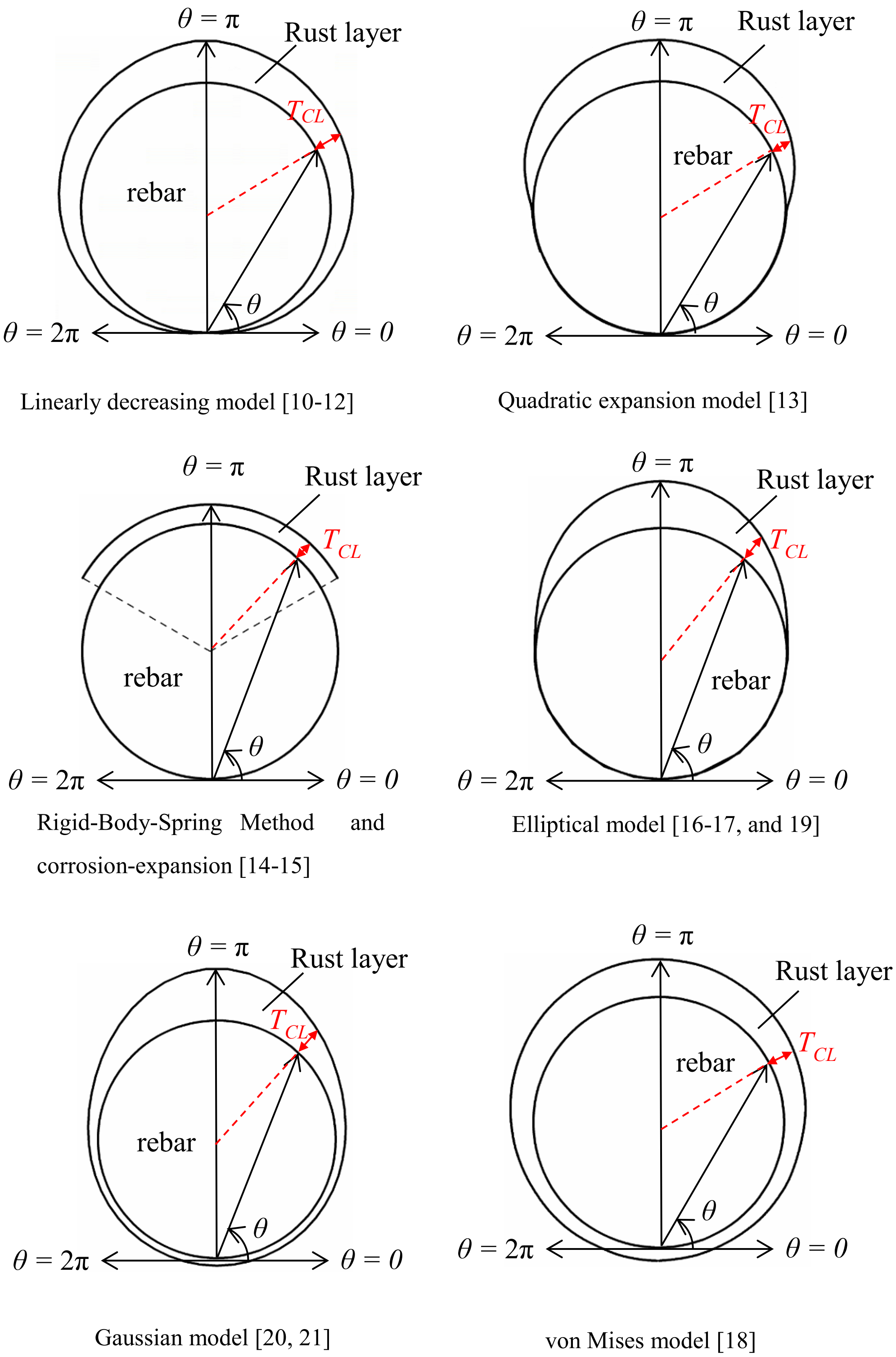

Figure 2. Distribution of rust layer around reinforcement with different models.

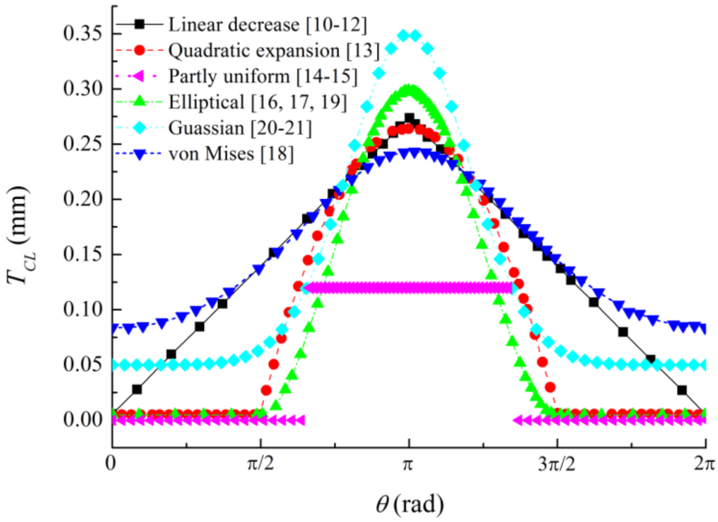

Figure 3. Thickness of rust layer T_{CL} versus θ angle with different models.

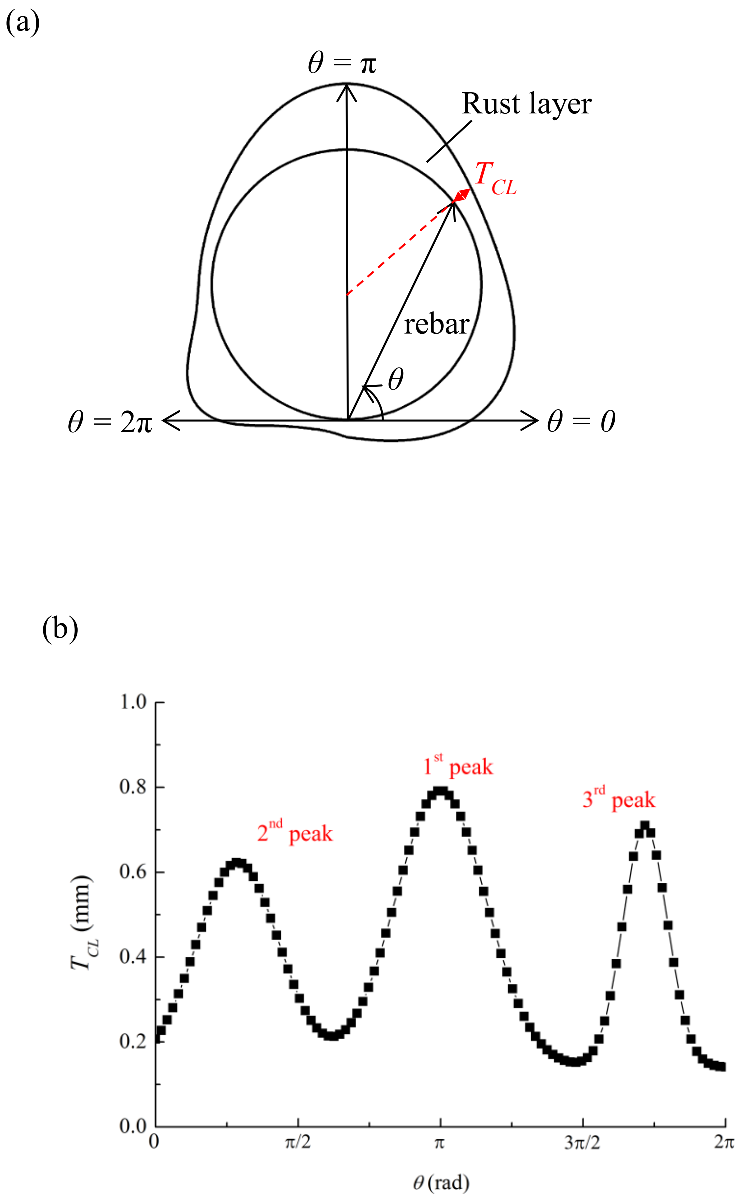

Figure 4. (a) Distribution of rust layer around reinforcement and (b) thickness of rust layer T_{CL} versus angle θ fitted with multiple-peak Gaussian function [21].

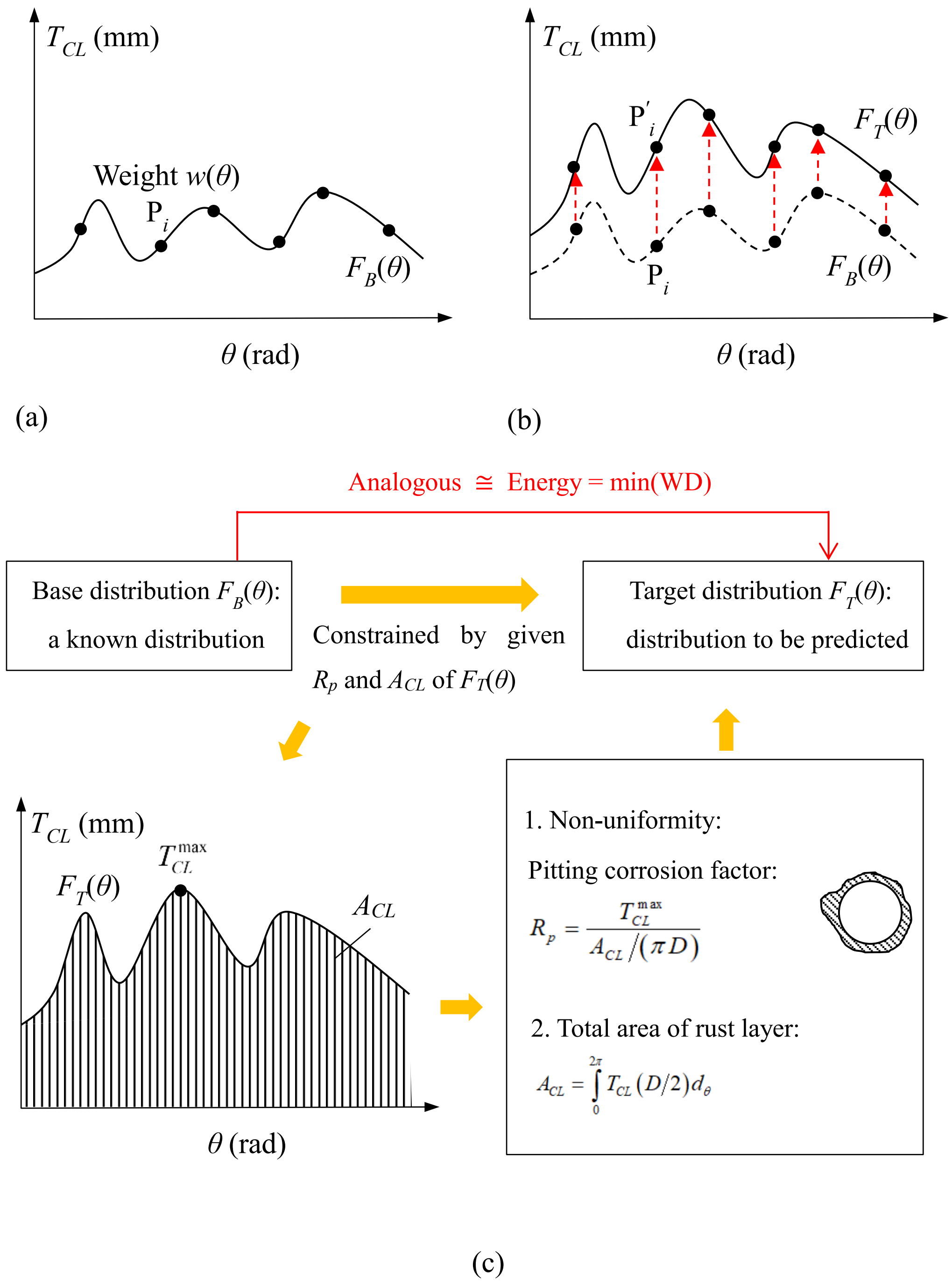

Figure 5. Problem to be solved in the WD-based method.

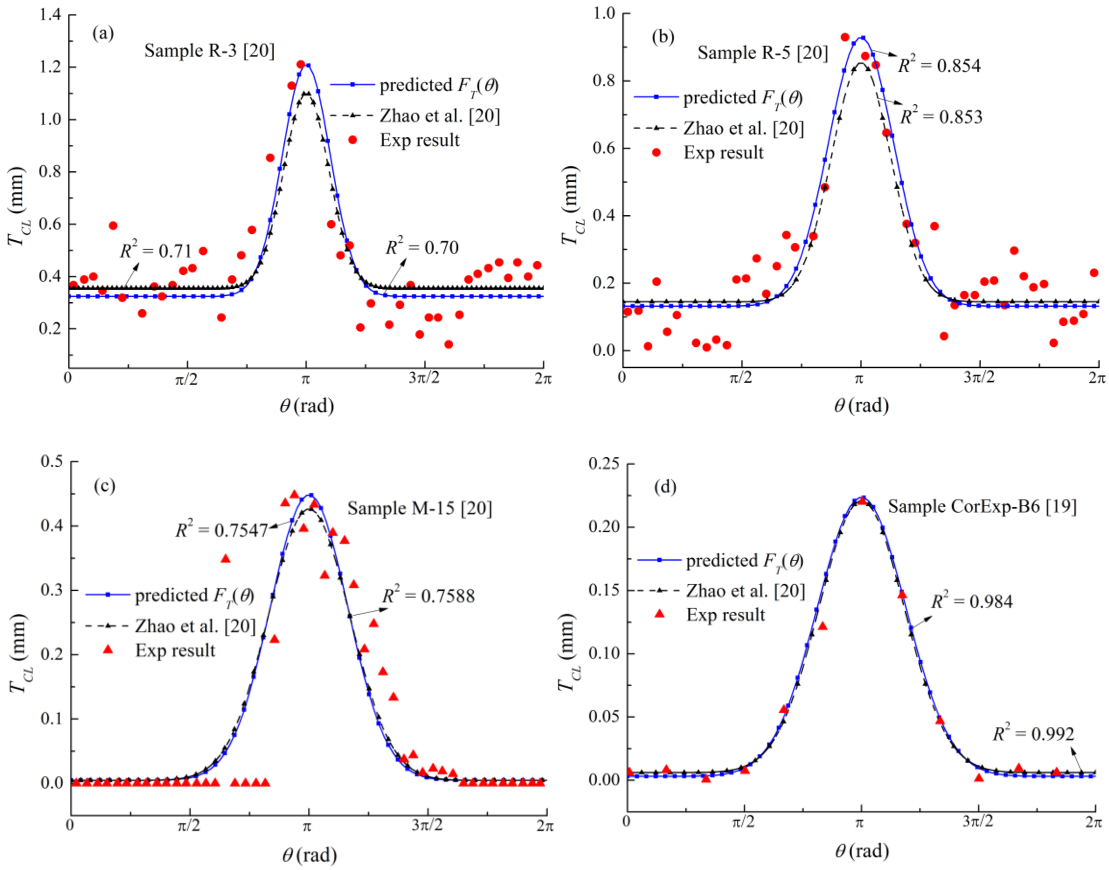

Figure 6. Predicted target distribution $F_T(\theta)$ of R-3, R-5, M-15 [20] and CorExp-B6 [19].

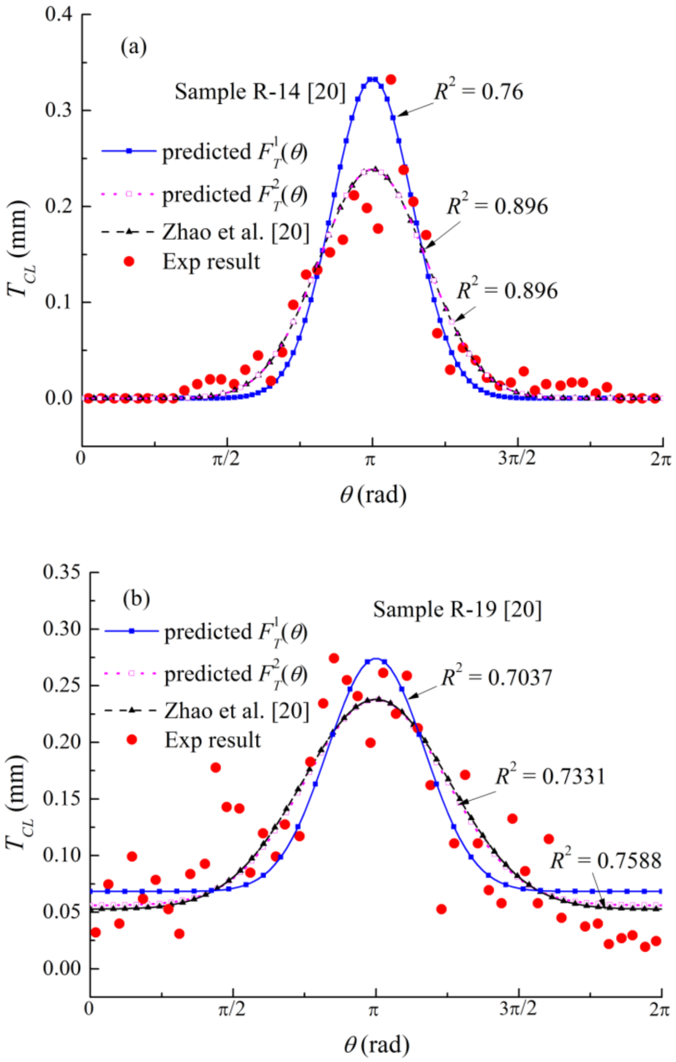

Figure 7. Predicted target distribution $F_T(\theta)$ of R-14 and R-19 [20].

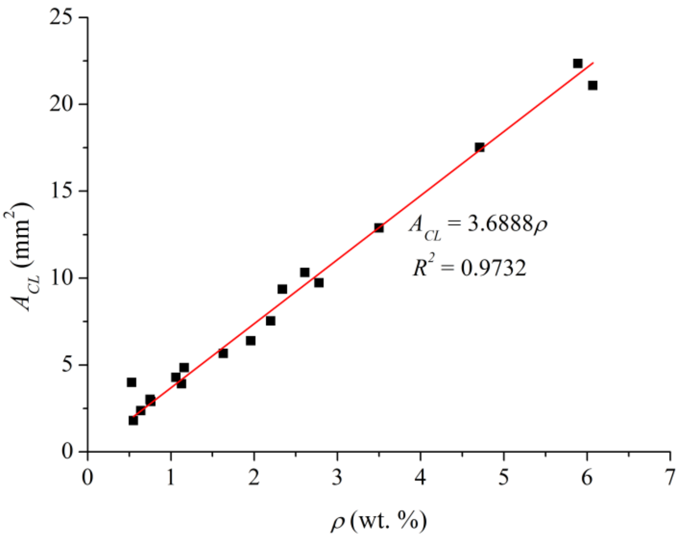

Figure 8. Fitted results of A_{CL} versus degree of corrosion ρ (wt. %).

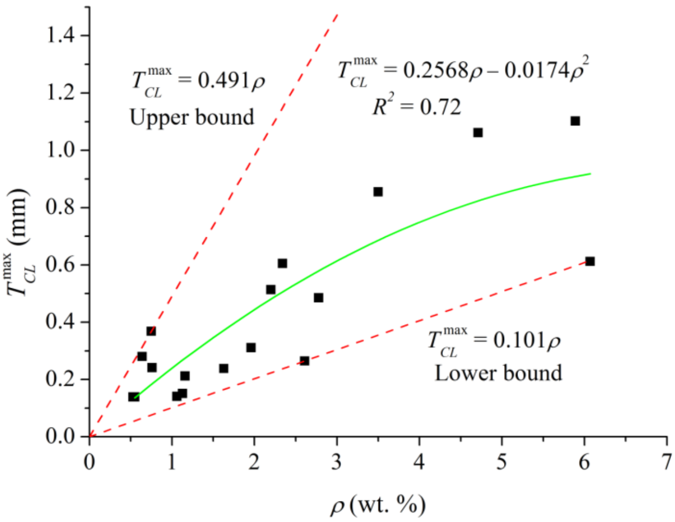

Figure 9. Fitted results of T_{CL}^{max} versus degree of corrosion ρ (wt. %).

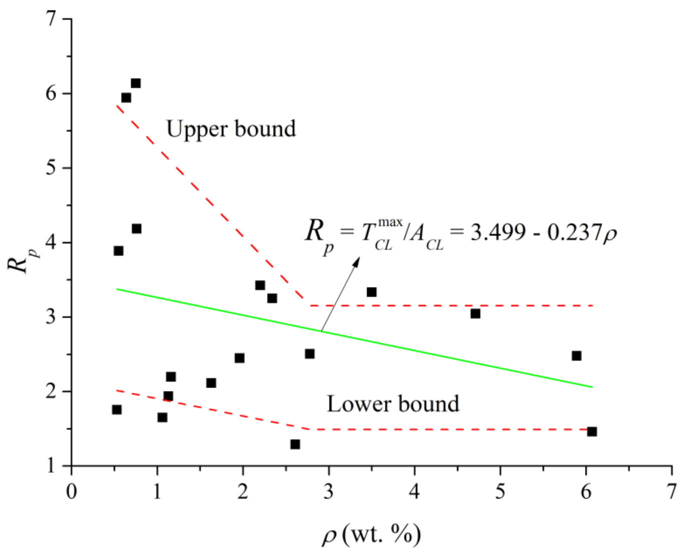

Figure 10. Fitted results of R_p versus degree of corrosion ρ (wt. %).